International Journal of Thermal Sciences 168 (2021) 107063

Contents lists available at ScienceDirect

International Journal of Thermal Sciences

journal homepage: www.elsevier.com/locate/ijts

Heat transfer characteristics of enhanced cooling tube with a helical wire under oscillatory flow in Stirling engine

Feng Xin [a,b,***], Minjie Yu [a], Wei Liu [a,*], Zhichun Liu [a,**]

[a] School of Energy and Power Engineering, Huazhong University of Science and Technology, Wuhan, 430074, China
[b] School of Energy and Power Engineering, Changsha University of Science and Technology, Changsha, 410114, China

ARTICLE INFO

Keywords:
Heat transfer performance
Enhanced cooling tube
Helical wire
Oscillatory flow
Stirling engine

ABSTRACT

Improving the heat transfer of cooler is favourable to reduce the cold end temperature and dead volume of Stirling engine. In this study, the effect of the implementation of a helical wire to a cooling tube of the reciprocating flow in Stirling engine was investigated numerically. The performance of helical wire with different geometric parameters and under different operating conditions were studied. The results show that the streamlines were helical and the fluid temperature homogeneity was improved. With the same size, the temperature drop of enhanced tube was 1.08–1.54 times as much as that of smooth tube. When obtaining the same outlet temperature, the diameter of smooth tube was 52% of that of enhanced tube with same tube length (for $p = 12.5$ mm, $h = 1.2$ mm, $d_0 = 1.6$ mm, $l = 180$ mm, $Re_{max} = 13{,}816$, $Re_\omega = 207$). Thus, the amount of smooth tube needed to increase to 3.7 times as much as that of enhanced tube. In another case (for $p = 12.5$ mm, $h = 1.2$ mm, $d_0 = 1.6$ mm, $d = 5$ mm, $Re_{max} = 13{,}816$, $Re_\omega = 207$), the length of smooth tube should be increased to above 2 times as much as that of enhanced tube with same tube diameter. Therefore, the tube with a helical wire could significantly enhance the heat transfer or decrease the size of cooler. Compared to smooth tube, the extra pressure drop by enhanced tube was accounts for no more than 0.6% of minimum pressure in Stirling engine (for $Re_{max} = 13{,}816$, $Re_\omega = 207$). It only accounted for 9.6–13.1% of the pressure drop of a regenerator. Therefore, the enhanced cooling tube with remarkable heat dissipation capacity and relatively low loss of pressure drop will present great application potential in Stirling engine.

1. Introduction

Stirling engine, an external-combustion engine, could be flexible for adopting many heat sources such as biomass, solar, geothermal energy, and industrial waste. Thus, Stirling engine is considered to be one of promising solutions to solve the problems caused by fossil fuels utilization. Moreover, Stirling engine is simple in construction, safe and quiet in operation with low emissions. Ideally, it can convert heat into mechanical work at Carnot efficiency [1,2]. With these advantages, the application of Stirling engine has attracted wide attention.

Extensive studies were performed to optimize the design for Stirling engine with an intention to obtain higher thermal efficiency, for example, the improvement on algorithm or model [3,4], the design on geometric parameters and operating parameters [5,6], the study on thermodynamic cycle [7,8], and so on. In addition, to optimize the design for Stirling engine, it is necessary to enhance the performance of engine from the view of structural innovation for each engine components. For a Stirling engine, the driving force is the expansion and compression of working gas, which is realized by heating and cooling of fluid. Accordingly, the heat exchangers included regenerator, heater and cooler played important roles in output power and efficiency of Stirling engine. Several studies investigated the flow and heat transfer characteristics of regenerator to improve its heat storage and release capacity [9,10], and studies regarding the structural innovation on heater to improve its heat transfer capacity were also reported [11,12].

Cooler, which is located between the compression chamber and the regenerator, is also an important heat exchanger in Stirling engine. The cooler transfers waste heat to system outside so that the compression process of cycle can be carried out under a lower temperature. Due to the low leakage loss, the cooling load in Stirling engine is almost twice as

* Corresponding author. .
** Corresponding author. .
*** Corresponding author. School of Energy and Power Engineering, Huazhong University of Science and Technology, Wuhan, 430074, China.
E-mail addresses: fengxin@csust.edu.cn (F. Xin), w_liu@hust.edu.cn (W. Liu), zcliu@hust.edu.cn (Z. Liu).

https://doi.org/10.1016/j.ijthermalsci.2021.107063
Received 16 August 2020; Received in revised form 27 April 2021; Accepted 10 May 2021
Available online 22 May 2021
1290-0729/© 2021 Elsevier Masson SAS. All rights reserved.

much as internal combustion engine with equivalent power [13]. Although many cooling devices have been widely studied in different areas [14–16], only a few researches reported the heat transfer and friction characteristic of cooler in Stirling engine. Dehghan et al. [17] and Kanzaka et al. [18] used shell and tube type heat exchanger as cooler in Stirling engine and investigated the reciprocating flow characteristic of fluid in cooler. Alfarawi et al. [19] used an aluminum finned type heat exchanger as a cooler of a gamma-type Stirling engine. The velocity, pressure and temperature distribution pattern and the velocity-pressure drop relationship for this cooler were studied in their study. Thombar et al. [20] calculated the total heat transfer coefficient of cooler, and found that the engine thermal efficiency decreased significantly when the coolant temperature increased. The above studies all focused on the flow and heat transfer regularity of fluid in a cooler. However, there is less research on the heat transfer enhancement of a cooler although it is extremely important to enhance the performance of Stirling engine.

If the heat exchange capacity of a cooler is enhanced, the waste heat will be released more sufficiently and the temperature difference between the cold source and the working fluid in cooler will be decreased. As a result, the compression process of a cycle will be carried out at a lower temperature and the efficiency of Stirling engine will be improved (see Fig. 1), or in the case of the same amount of heat exchange, the volume of the cooler can be effectively reduced after enhancing the heat exchange capacity of the cooler. Thus, the dead volume of Stirling engine will be reduced and the output power of per unit mass of working medium will be increased. Water, with strong heat transfer capacity, is usually used as the cooling liquid outside of tube. However, the fluid inside of tube is working gas, which has relatively weak heat transfer capacity compared with fluid outside (i.e., water). This implies that the thermal resistance of cooling tube is mainly from convection coefficient inside tube. Thus, it is necessary to enhance heat transfer between the working gas and the cooling wall.

Nowadays, the traditional enhanced heat transfer technologies based on steady flow have been widely studied [21,22]. Some theories, such as field synergy [23,24], entropy generation [25,26] and exergy destruction [27], were applied to analyze the heat transfer enhancement effect. Some methods, such as artificially roughened surface [28], various tube inserts [29–31] or special section tube [32], were developed to enhance the heat transfer of heat exchange tubes. However, the results on the heat transfer enhancement performance for unidirectional steady flow might not be suitable for the Stirling engine coolers, since the fluid is in a reciprocating oscillating flow state.

The velocity, pressure, temperature and physical parameters of fluid all change with time in Stirling engine. At present, rare studies regarding

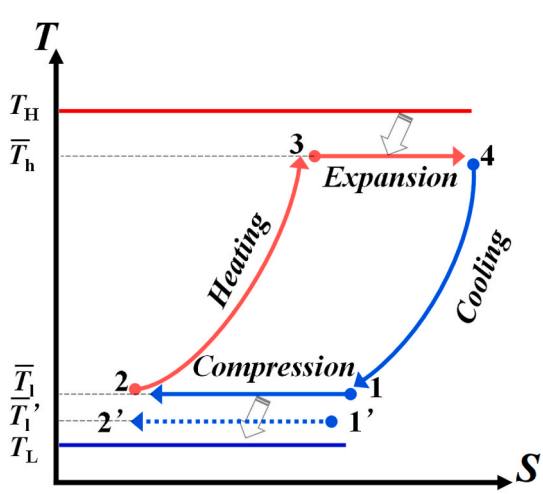

Fig. 1. Schematic diagram of the Stirling cycle (1-2-3-4 Stirling cycle; 1′-2′-3-4 Stirling cycle after enhancing the heat exchange of the cooler).

the heat transfer enhancement for oscillatory flow were conducted. Kuosa et al. [33] investigated the heat transfer enhancement by means of a few circumferential slots inside the cooling tubes or non-circular cross-section conduits compared to the smooth circular tubes under the oscillatory flow. However, this study was based on the early empirical formulas, and the analyses of the velocity field, temperature field and pressure field were lacked. Qi et al. [34] studied the heat transfer characteristic of cooler with different kinds of fins for free-piston Stirling engine. However, the overall heat transfer enhancement needed to be further improved as the *PEC* was less than 1. Compared to the cooler with fins, the heat pipe radiant cooler in Stirling engine proposed by Tang et al. [35] has a better overall heat dissipation capacity. Nevertheless, the compactness of the Stirling engine was weakened and the real-world applications were restricted because of the radiant plates in this type of cooler. Accordingly, it is essential to further study the heat transfer enhancement of cooling tubes for Stirling engine under oscillatory flow.

In addition, the performance evaluation method of enhanced cooling tube under reciprocating oscillating flow was also needed to further research. Many assumptions for the previous Performance Evaluation Criterion (*PEC*) are based on steady flow, which are not suitable for reciprocating oscillatory flow. Moreover, the velocity of flow was nearly 0 m/s when the velocity reversal occurred in oscillatory flow, hence causing an extremely huge resistance coefficient. However, this resistance coefficient was not caused by the helical wire, but resulted from the velocity reversal of fluid in cooling tube which was derived from the compression and expansion of working medium in compression chamber and expansion chamber of Stirling engine. Therefore, it is necessary to explore the new performance evaluation of enhanced tube under reciprocating oscillating flow in Stirling engine.

The methods of heat transfer enhancement are generally divided into two groups: passive methods and active methods. Passive methods are much more efficient than active methods due to their simpler performance and easily utilization in modern thermal equipment [36]. Among various passive methods, the disturbing devices with helical-structure are commonly used because of its simple structure and generation of swirl flows [37]. Compared with other helical-structure disturbing devices, the pressure drop of helical wire is smaller and it can be added to equipment easily and its costs is relatively low too. At present, heat exchange tubes inserted with helical wires was widely used in enhancing heat transfer field [38], which have been demonstrated an excellent performance of enhanced heat transfer for unidirectional laminar flow [37], oscillatory baffled reactors [39,40], etc. Garcia et al. [41]examined the heat transfer enhancement performance through helical wire inserts in a heat exchanger under unidirectional laminar, transition and turbulent flow. An increase in heat transfer was reported by using the helical wire inserts. Zimparov et al. [42] compared the thermal and hydraulic performance of twisted tapes, helical wires and helically coiled ribbons inside a heat-exchanger in unidirectional turbulent flow regions. The results showed that the helical wires were more efficient and useful under high Reynolds number conditions.

In this work, a helical wire was developed and employed in Stirling engine cooling tube with an intention to enhance its heat dissipation performance under reciprocating oscillatory flow. The helical wire was be chosen because it is suitable for heat transfer enhancement of both forward flow and reverse flow with large velocity magnitude, owing to its helical structure and small pressure drop. The flow and heat transfer mechanism in this enhanced tube under reciprocating oscillatory flow was studied by CFD numerical simulation. Different from the previous evaluation on enhanced heat transfer, such as *PEC* [43,44], the advantages of enhanced tube were evaluated by the decrease of outlet temperature or the reduction of cooler size. This evaluation method can directly reveal the benefit of enhanced tube for Stirling engine. Further, the cost of enhancing heat transfer caused by the helical wire for cooling tube was also discussed by pressure drop loss in this study.

2. Physical and mathematical models

2.1. Physical model

The structural diagram of a cooling tube with a helical wire was shown in Fig. 2. Fig. 2 (a) and (c) show the sectional views perpendicular to circular tube and helical wire, respectively. The cross-section shape of a helical wire is part of a circle (Fig. 2 (c)). The ends of wire are straight and the middle part is helical. The flow and heat transfer of working fluid in a smooth cooling tube were also investigated to evaluate the enhanced heat transfer performance of cooling tube with a helical wire. The specific geometric parameters of cooling tubes were shown in Table 1.

2.2. Mathematical model

According to the general mathematical model of oscillatory flow of viscous fluid, body forces and internal heat sources are neglected. The k-ω model and shear-stress transport (SST) k-ω model are commonly used in engineering applications for unsteady-state turbulent flow and the latter one is more applicable for this kind of oscillatory flow [28,44]. Thus, the SST k-ω model was employed in this work. The working fluid in the simulation was helium (He). The physical properties varied with the working conditions. The change regularity of temperature, velocity and pressure for fluid with time and space was studied based on transient reciprocating flows.

2.2.1. Governing equation

Continuity equation:

$$\frac{\partial \rho}{\partial t} + \nabla \cdot (\rho \vec{u}) = 0 \tag{1}$$

Momentum equation:

$$\rho \cdot \frac{\partial \vec{u}}{\partial t} + \nabla \vec{u} \cdot (\rho \vec{u}) = -\nabla P - \frac{2}{3}\nabla[\mu(\nabla \cdot \vec{u})] + \nabla \cdot \left[\mu(\nabla \vec{u})^T\right] + \nabla \cdot [\mu(\nabla \vec{u})] \tag{2}$$

Energy equation:

$$\rho c_p \cdot \frac{\partial T}{\partial t} + \rho c_p \vec{u} \cdot \nabla T = \nabla[\lambda(\nabla \cdot T)] + \left[\frac{\partial P}{\partial t} + \vec{u} \cdot \nabla P\right] + \Phi \tag{3}$$

The turbulence kinetic energy equation:

$$\frac{\partial}{\partial t}(\rho k) + \frac{\partial}{\partial x_i}(\rho k u_i) = \frac{\partial}{\partial x_i}\left((\mu + \sigma_k \mu_t)\frac{\partial k}{\partial x_i}\right) + \widetilde{P}_k - \beta^* \rho k \omega \tag{4}$$

The specific dissipation rate equation:

$$\frac{\partial}{\partial t}(\rho \omega) + \frac{\partial}{\partial x_i}(\rho \omega u_i) = \frac{\partial}{\partial x_i}\left((\mu + \sigma_\omega \mu_t)\frac{\partial \omega}{\partial x_i}\right) + \alpha \rho S^2 - \beta \rho \omega^2 + 2(1 - F_1)\rho \sigma_{\omega 2}\frac{1}{\omega}\frac{\partial k}{\partial x_i}\frac{\partial \omega}{\partial x_i} \tag{5}$$

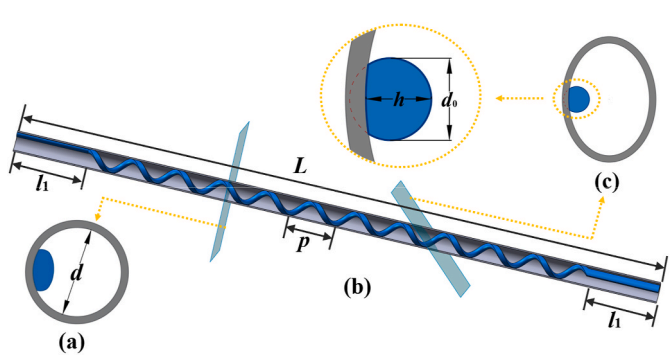

Fig. 2. The schematic diagram of a cooling tube with a helical wire.

Table 1
The structural parameters of cooling tubes.

Structural parameters/mm	l	d	l_1	p	p/d	d_0	d_0/d	h	h/d
Enhanced tube	180	5	20	12.5	2.5	1.4	0.28	0.6	0.12
				15	3	1.5	0.3	0.8	0.16
				17.5	3.5	1.6	0.32	1.0	0.2
				20	4	1.7	0.34	1.2	0.24
				22.5	4.5	1.8	0.36	1.4	0.28
Smooth tube	180	5	–	–	–	–	–	–	–
	270	4							
	360	3							
	450	2							
	540	1							

where the meaning of each symbol in above formulas were interpreted in literature [45].

2.2.2. Boundary conditions

The hot and cold ends of cooling tube for Stirling engine are connected to the regenerator and the compression chamber of Stirling engine, respectively. The working medium flows from the regenerator to the compression chamber during entry process, while it flows to the opposite direction during return process. The velocity magnitude and pressure change from time to time, and the flow direction reverse one time interval of 180°. For cooling tube, in the entry process, the hot end is the inlet, and the cold end is the outlet. In the return process, the cold end is the inlet and the hot end is the outlet. The boundary conditions of hot end, cold end and wall surface are shown in Fig. 3, the detailed settings of which are as following:

Hot end is set as velocity boundary condition. The velocity change regular is shown in formular (6). For different $Re_{\max}$ and Re_ω, the $u_{\mathrm{m,\,max}}$ and ω are different. The hot end temperature is set as 398 K in entry process.

$$u = u_{\mathrm{m,max}} \sin(\omega t) \tag{6}$$

Cold end is set as pressure boundary condition. The pressure change regular is shown in formular (7). The cold end temperature is set as 302 K in return process.

$$P = P_0 - P_1 \cos(\omega t) \tag{7}$$

The wall is set as constant wall temperature boundary body condition. The wall temperature is set as 298 K.

2.3. Parameter definition

In the oscillatory flow, there are two kinds of Reynolds number, which can be expressed as following:

$$Re_{\max} = \frac{\rho u_{\mathrm{m,max}} d}{\mu} = \frac{u_{m,\max} d}{\nu} \tag{8}$$

$$Re_\omega = \frac{\rho \omega d^2}{\mu} = \frac{\omega d^2}{\nu} \tag{9}$$

where the $Re_{\max}$ is based on the amplitude of the bulk mean velocity, and it is similar to the Reynolds number in steady flow. The Re_ω is a dimensionless frequency which represents the ratio of the time scale of viscous dissipation to the time of one cycle. The expressions of heat transfer coefficient, the Nusselt number and friction factor are as following:

$$h = \frac{q}{T_{\mathrm{w}} - T_{\mathrm{m}}} \tag{10}$$

$$Nu = \frac{hd}{\lambda} \tag{11}$$

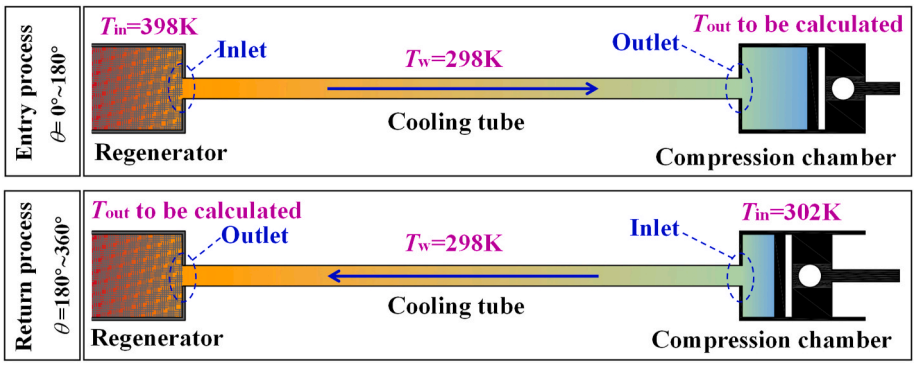

Fig. 3. The schematic diagram for the flow of working medium in a cooling tube.

$$f = \frac{|\Delta P|}{(l/d)\rho u_m^2/2} \tag{12}$$

where T_w represents the temperature of wall, T_m represents the average temperature of working fluid, and q denotes the average heat flux of wall. The u_m represents the mean velocity of fluid. In the formular (12), the absolute value of pressure difference was used because the fluid is in a back-and-forth flow alternately in the oscillatory flow.

2.4. Model validation

The fluid domain was discretized by full hexahedral grid, as shown in Fig. 4. To verify the accuracy of numerical solutions, grid independence tests with different grid number 599250, 1,651,762, 2,947,698, and 3,858,102 were performed, respectively. The results show that the deviation of calculated values for the grids system of 2,947,698 and 3,858,102 elements was 1.084% for heat flux and 1.11% for velocity. This suggests that the grid system with about 2.9 million elements was adequately dense for the numerical simulation, which was applied in the following simulation.

For the transient alternating flow, it would spend some time from the calculation beginning to the stable change regularity of flow. To acquire accurate calculation results, the stability verification of the flow change regularity was carried out. The results indicate that the deviation of the fourth and fifth cycle was about 0.58% for heat flux and 0.17% for velocity. Thus, considering a compromise of time and solution precision, the flow change regularity was considered stable after calculating four cycles.

The model validation was also carried out by comparing with the experimental and theoretical analysis results [46,47]. The detailed data are shown in Fig. S1 (a)~(l) in Supporting Information. As shown, the simulation results agreed well with the experimental results and analytical solutions in literatures, suggesting that the model used in this work was reliable.

3. Results and discussion

3.1. Analysis of heat transfer characteristics in cooling tube

3.1.1. Flow structure

The flow was in entry and return process for $\theta = 0°\sim180°$ and $\theta = 180°\sim360°$, respectively, while it was in the transition for $\theta = 0°$ and $\theta = 180°$. The fluid flow in smooth tube was undisturbed and the streamlines were straight. However, in the enhanced tube, the flow of fluid became helical with the disturbance of wire.

Fig. 5 shows local streamlines in the middle part of enhanced tube for representative phase angle. As shown, when the phase angle was equal to 90° or 270°, a large flow velocity of fluid occurred. The flow direction of fluid at $\theta = 90°$ which is in entry process was opposite to that at $\theta = 270°$ which is in return process. There was a radial velocity component in enhanced tube, the direction of which was opposite for $\theta = 90°$ and $\theta = 270°$. Thus, the rotation direction of streamlines at $\theta = 90°$ was opposite to that at $\theta = 270°$. For the entry (e.g., $\theta = 90°$) or return (e.g., $\theta = 270°$) process, the axial velocity component of fluid in the core flow zone was large, while it was small in the boundary flow zone because of the hamper of viscous resistance near the wall surface. Thus, the helical pitch of streamlines in the core flow zone was large and it was small in the boundary flow zone.

When the phase angle was equal to 0°, the flow was in the transition process, the entry and return streamlines occurred simultaneously. The streamline near the core area mostly flowed from inlet to outlet (i.e., entry process direction), while the streamline near the wall mostly flowed from outlet to inlet (i.e., return process direction). The overall velocity of the fluid in the core area was very small, especially the axial velocity component, while the velocity of the fluid in the boundary area was relatively large. This is because the velocity magnitude was supposed to 0 m/s when $\theta = 0°$ as the flow of fluid was in the transition stage from return process to entry process. In the core area, the fluid velocity was greatly influenced by the inlet fluid velocity, and the velocity magnitude was close to 0 m/s. The flow direction began to turn to entry

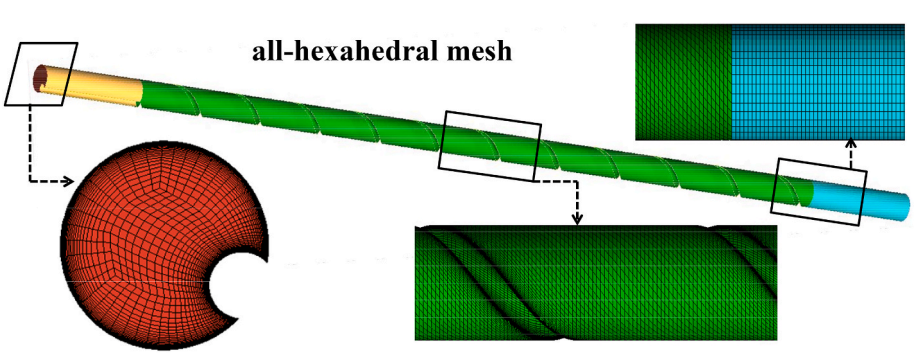

Fig. 4. The grid generation for the computation domain of enhanced tube.

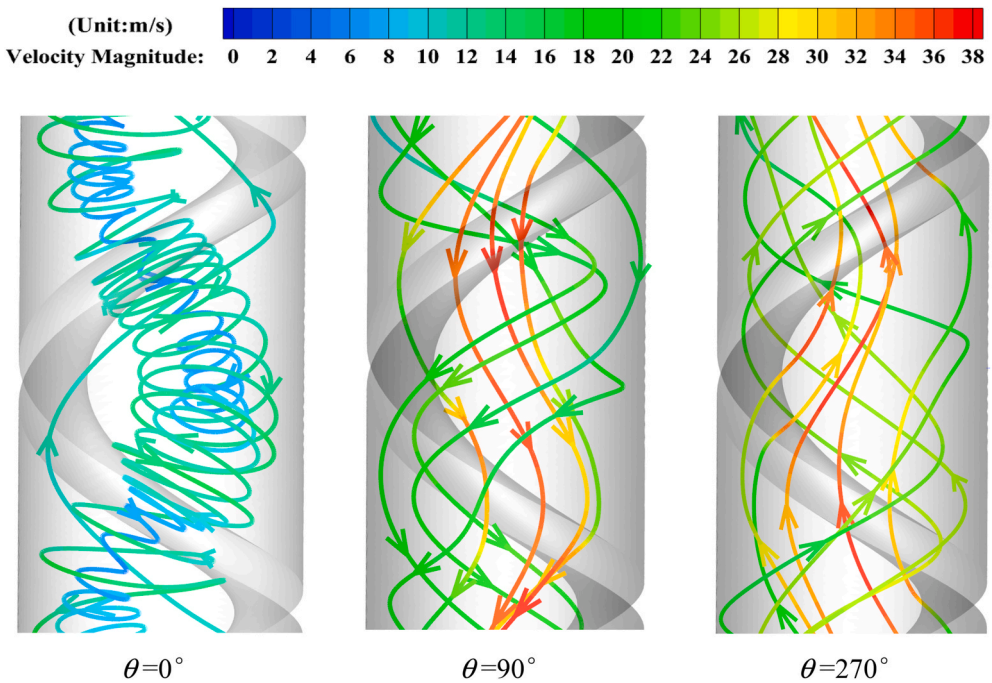

Fig. 5. The local streamlines in the middle part of enhanced tube.

direction. In the border region, the flow of fluid was greatly influenced by the previous flow in the cooling tube due to the influence of the viscous force and inertial force. The velocity magnitude was slightly bigger than 0 m/s and the flow direction still was in return process.

Fig. 6 shows the velocity contour plots of cooling tube in center axial cross section. It can be observed that the boundary velocity (u) was the most important factor for affecting the velocity contour plots of the fluid in the cooling tube. When the phase angle was 0°, the boundary velocity magnitude was 0 m/s (see formula (6)). The velocity of fluid was very small in smooth tube and enhanced tube compared with velocity in other phase angles. When the phase angle was 90° or 270°, the boundary velocity was $u_{m,max}$ (see formula (6)). The velocity in the cooling tube was the maximum during a cycle. By comparing Fig. 6 (a) and (b), it was found that the velocity in the enhanced tube was overall larger than that in the smooth tube, which was due to the disturbance of helical wire. For the enhanced tube, when the phase angle was 0°, there were some areas far away from helical wire with the velocity near 0 m/s. These areas were the vortex cores. When the phase angle was 90°, the fluid flowed from the left end (connected to the regenerator end) to the right end (connected to the expansion chamber end). At this moment, the fluid velocity in the left region of the helical wire was relatively large, while the fluid velocity in the right region of the helical wire was relatively small. When the phase angle was 270°, the fluid flowed from the right end (connected to the expansion chamber end) to the left end (connected to the regenerator end), and the fluid velocity in the right region of the helical wire was relatively large, while the fluid velocity in the left region of helical wire was relatively small. In summary, the velocity near the upstream flow side was larger than that in the downstream side for the fluid surrounding the helical wire area.

Fig. 7 shows that the radial component velocity contour plots with

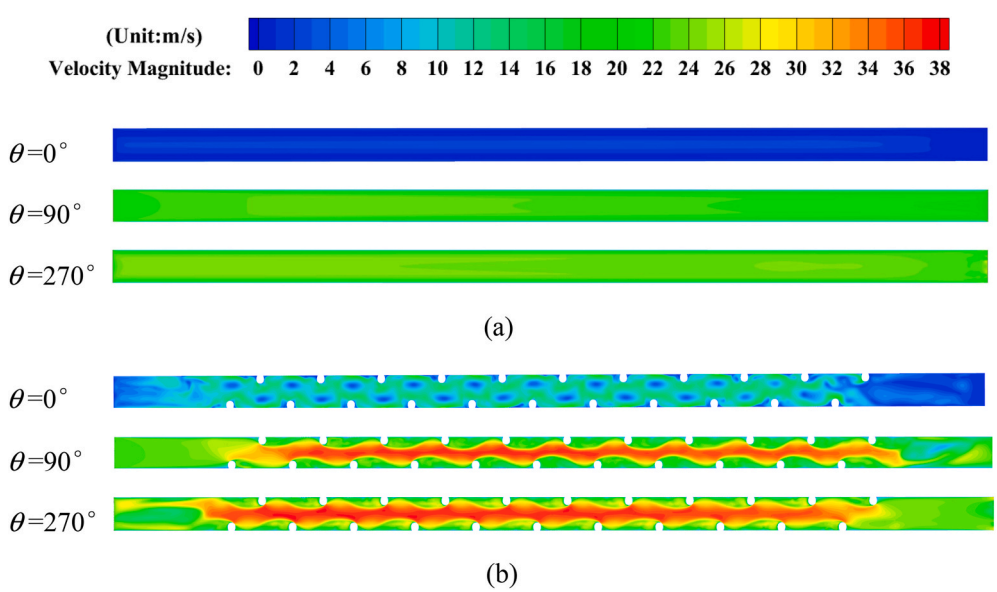

Fig. 6. The velocity contour plots of cooling tube in center axial cross section: (a) smooth tube; (b) enhanced tube.

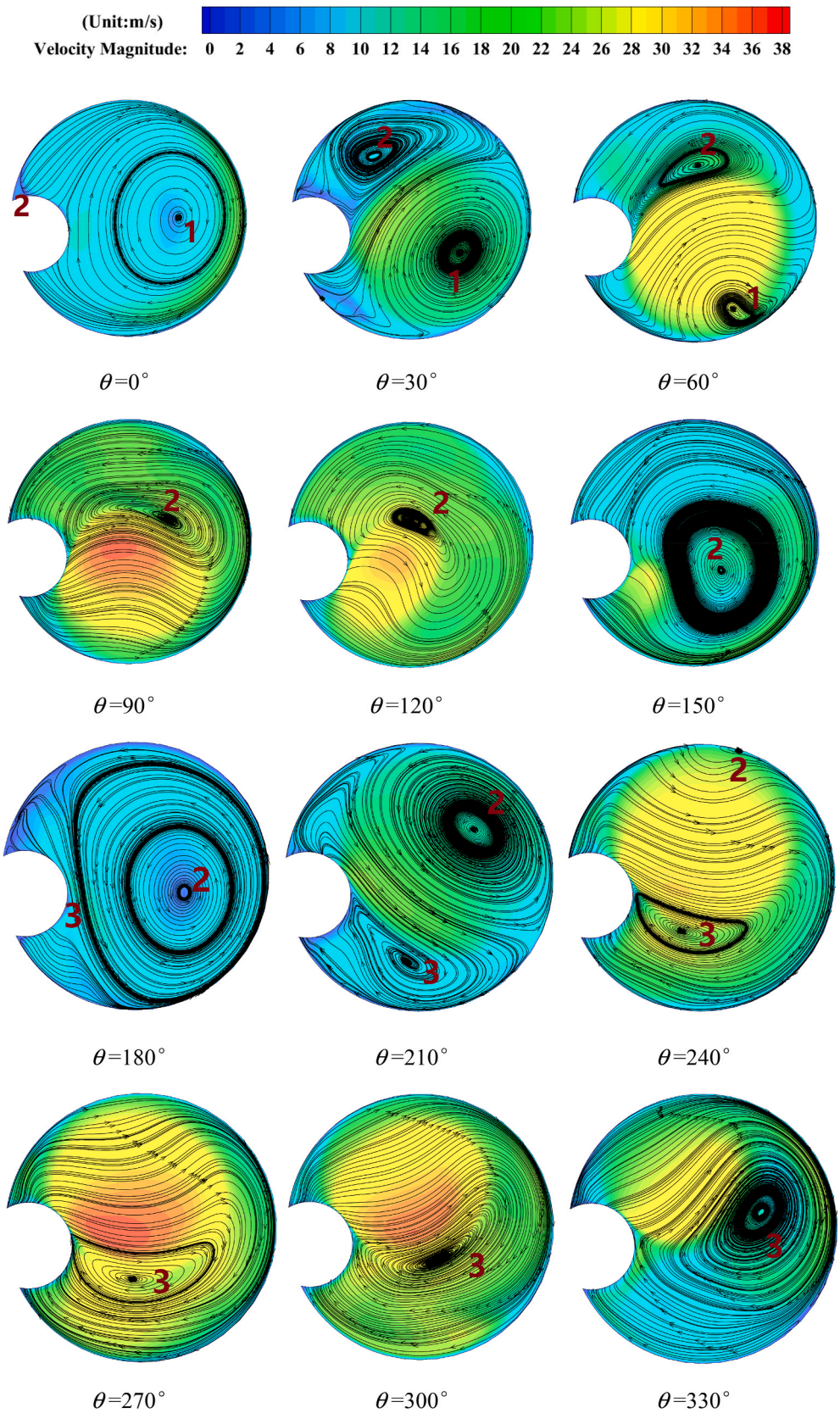

Fig. 7. The velocity contour plots with streamlines of enhanced tube in center radial cross section (z = 90 mm).

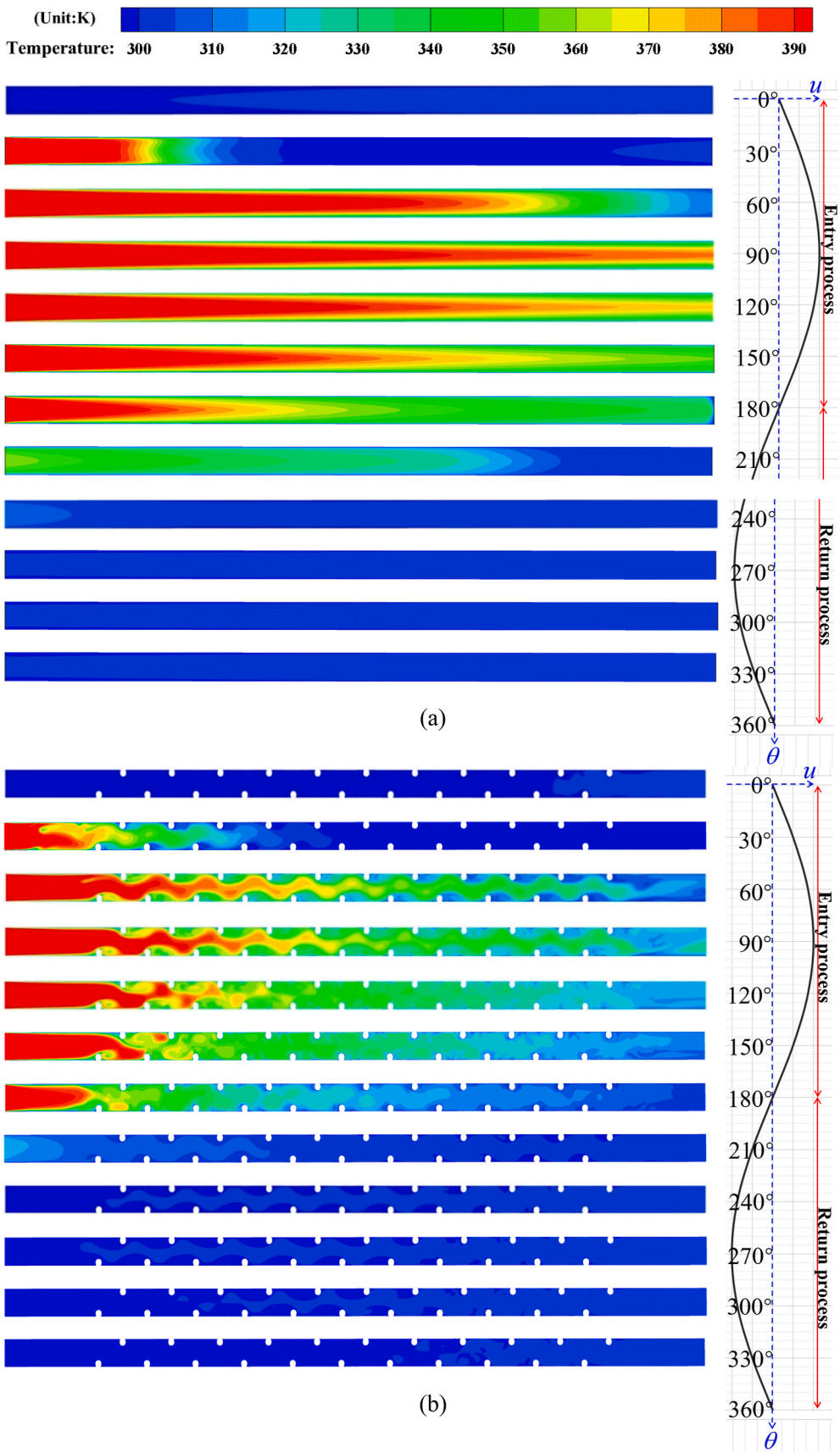

Fig. 8. The temperature contour plots of cooling tube: (a) smooth tube in center axial cross section; (b) enhanced tube in center axial cross section; (c) smooth tube (left part) and enhanced tube (right part) in different radial cross sections.

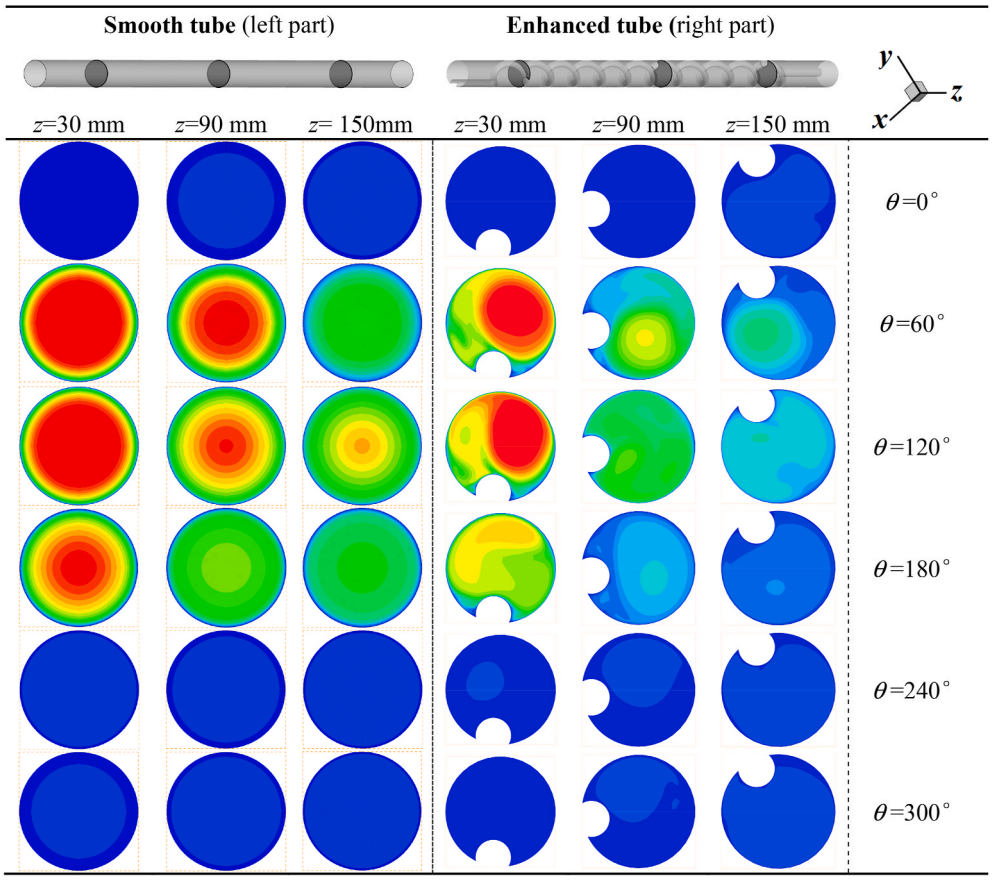

(c)

Fig. 8. (*continued*).

streamlines in center radial cross section ($z = 90$ mm). It can be seen that the flow vortexes were generated in the radial section for enhanced tube. At different moments, the state of vortexes was varied in view of number, size and position. In order to descript the change of vortexes, the different vortexes were named (shown in Fig. 7), and their change regular can be summarized as following: (i) when the phase angle was equal to 0°, there were a large vortex No. 1 in the center of cross section. At the same time, an inconspicuous small vortex No. 2 began to appear near the upper side of the helical wire; (ii) when the phase angle was in 0°~90°, the flow of fluid in cooling tube was in the acceleration stage of entry process. The No. 1 large vortex gradually moved to the lower side of the cross section, and gradually became smaller until it disappeared. The No. 2 small vortex gradually grew up and moved toward the center of cross section; (iii) when the phase angle was in 90°~180°, the flow of fluid in cooling tube was in the deceleration stage of entry process. The No. 2 vortex grew further and moved toward to the central part of cross section; (iv) when the phase angle was equal to 180°, besides the large vortex No. 2 which was still in the center part of cross section, a small vortex No. 3 gradually formed near the helical wire; (v) when the phase angle was in 180°~270°, the flow of fluid in cooling tube was in the acceleration stage of return process. The large vortex No. 2 moved upward and gradually became smaller until it disappeared. The No. 3 small vortex gradually grew up and moved toward the center of cross section; (vi) when the phase angle was in 270°~360°, in which the 360° also was same as 0°, the flow of fluid in cooling tube was in the deceleration stage of return process. The No. 3 vortex grew further and moved toward to the central part of cross section. In the next cycle, the same change regular of vortex repeated. The velocity contour plots with streamlines of enhanced tube in radial cross section for $z = 30$ mm and $z = 150$ mm at different phase angles were shown in Fig. S2 in Supporting Information. It can be seen that the changes of vortexes with phase angle at different radial sections displayed similar regular.

In the enhanced tube, the alternate forming, change and vanishing of vortices generated by the helical flow promoted the fluid exchange between boundary and core regions, and the flow boundary layer became thinner. As a result, the thermal boundary layer was thinned and the heat transfer was enhanced. Under the same boundary conditions, the heat of fluid in enhanced tube can be released more quickly compared with that in smooth tube. Thus, the temperature of fluid entering the compression chamber was lower and the efficiency of the Stirling engine could be improved.

3.1.2. Temperature field

Fig. 8 shows the temperature contour plots of cooling tube in center axial section (Fig. 8 (a) and (b)) and different radial sections (Fig. 8 (c)) for some specific phase angles. For both smooth and enhanced tubes (Fig. 8 (a) and (b)), in entry process, the temperature of fluid in the cooling tube varied significantly at different phase angles. However, in the return process, the temperature contour plots are basically dark blue, and the overall temperature of fluid distributes uniformly. This is mainly due to temperature difference between the inlet fluid and wall. In entry process, the inlet temperature of fluid is 398 K and the wall temperature is 298 K. The large temperature difference (100 K) contributes to the obvious cooling effect of wall for fluid. However, in return process, the inlet temperature of fluid is 302 K and the wall temperature also is 298 K. Such small temperature difference (4 K) makes the cooling effect of wall inconspicuous. By comparing the temperature clouds at different phase angles (Fig. 8 (a) or (b)), it can be observed that the inlet velocity (u) of fluid significantly affected the temperature distribution of fluid. The cooling effect of tube wall on working fluid increased with the

decrease of inlet velocity, since the working fluid has more time to be cooled by the tube wall at lower velocity.

Compared Fig. 8 (a) with (b) or compared Fig. 8 (c) left part with right part, it can be seen that the heat transfer in enhanced tube was much better than that in smooth tube. For instance, when the phase angle was 60°, for smooth tube, the average temperature of the central axis section was 367.7 K, and the average temperature of the central radial section was 365.4 K. While for enhanced tube, the average temperature of the central axis section was 347.8 K, and the average temperature of the central radial section was 336.6K. When the phase angle was 120°, the former were 373.3 K and 362.8 K respectively, while the latter were 347.6K and 339.1K respectively. It means that the fluid in the enhanced tube can be better cooled under the same conditions. Moreover, compared with smooth tube, the temperature uniformity of fluid in the enhanced tube was better as well. For instance, when the phase angle was 120° at $z = 90$ mm (in Fig. 8 (c)), the temperature difference of fluid in the core flow region and near the boundary flow region was large for smooth tube, while the temperature distribution was apparently uniform for enhanced tube at the same case.

The much superior cooling performance for enhanced tube is because that the wire insert created a helical disturbance to the fluid flow and longitudinal swirl was formed, which promoted the mixture of boundary fluid with core fluid. Thus, large temperature gradient and thin temperature boundary layer near wall surface was formed. Moreover, it can be seen from Fig. 8 (b) that the heat transfer performance in the middle part of enhanced tube with a helical wire was significantly better than that in the ends part with straight wire.

From Fig. 8 (b), it can be seen that the temperature in the fluid region nearby wire facing flow direction was higher than that facing away flow direction. This is because the velocity of fluid nearby helical wire in the upstream flow side was larger than that in the downstream side (seeing Fig. 6(b)). The velocity magnitude of fluid was large near the region of upstream flow side of helical wire, which resulted in less time to be cooled for fluid by wall. However, the velocity magnitude of velocity is relatively small near the region of downstream flow side of helical wire, hence owning more time to be cooled for fluid by wall.

Compared the right part of Fig. 8 (c) with Fig. 7, Fig. S2 (a) and (b), it can be seen that the fluid temperature near the newly formed vortex was significantly lower than that near the gradually vanished vortex. The velocity magnitude of fluid near the newly formed vortex was relatively small, so there is more time to be cooled for fluid by wall. While the velocity magnitude of fluid near the gradually vanished vortex is relatively large, so there is less time to be cooled for fluid by wall. In general, for the entry process, the high temperature region on the temperature contour plots was basically the high velocity region on the velocity contour plots, while this regular was not obvious for the return process. Because the temperature difference between the inlet and the wall temperature is too small (4 K), so the temperature contours all is blue low temperature region.

Moreover, the wall heat flux plots of cooling tube for different phase angles were shown in Fig. S3 in Supporting Information to express the heat transfer characteristics in the cooling tube better.

3.1.3. The heat transfer coefficient and Nusselt number

Fig. 9 shows the transient and average heat transfer coefficient change with Reynolds number. Fig. 10 shows the transient and average Nusselt number change with Reynolds number. It can be seen that the transient heat transfer performance of the cooling tube changed all the time in a flow cycle. The moment in which the maximum heat transfer coefficient and the maximum *Nu* value of the enhanced tube occurred was slightly behind the smooth tube. The transient heat transfer coefficient and *Nu* number of the cooling tube increased with the Re_{max} and Re_{ω} number. The increasing amplitude of the enhanced tube is significantly larger than that of the smooth tube. The effect of Re_{max} and Re_{ω} number on the heat transfer coefficient and *Nu* number was more remarkable in the moments of large velocity (i.e., $\theta = 90°$ or $\theta = 270°$) for smooth tube compared with the reverse moment (i.e., $\theta = 0°$ or $\theta = 180°$) of fluid. However, the above-mentioned regular for enhanced tube was not obvious. The average heat transfer coefficient and average *Nu* number of the cooling tube increased with the increase of Re_{max} and Re_{ω} number for both smooth tube and enhanced tube. Within the dimensionless parameter range in this study, the increase regular is approximately linear relationship, and the increase range of the enhanced tube is significantly larger than that of the smooth tube.

3.1.4. Outlet temperature

The outlet temperature of fluid can intuitively reflect the cooling effect of cooling tube. The low outlet temperature of cooling tube meant the low inlet temperature of compression chamber. Consequently, the cold end temperature of thermodynamic cycle for Stirling engine was decreased and the engine efficiency was increased (see Fig. 1). The transient variation regularity of outlet temperature for smooth tube and enhanced tube with different helical pitches was shown in Fig. 11. As shown, the flow process was divided into two processes, i.e., the entry process and the return process. Each process was divided into two stages, corresponding to the transition section and stability flow direction section, respectively.

(1) In stage I, fluid began to flow from the regenerator end to compression chamber end along the cooling tube. However,

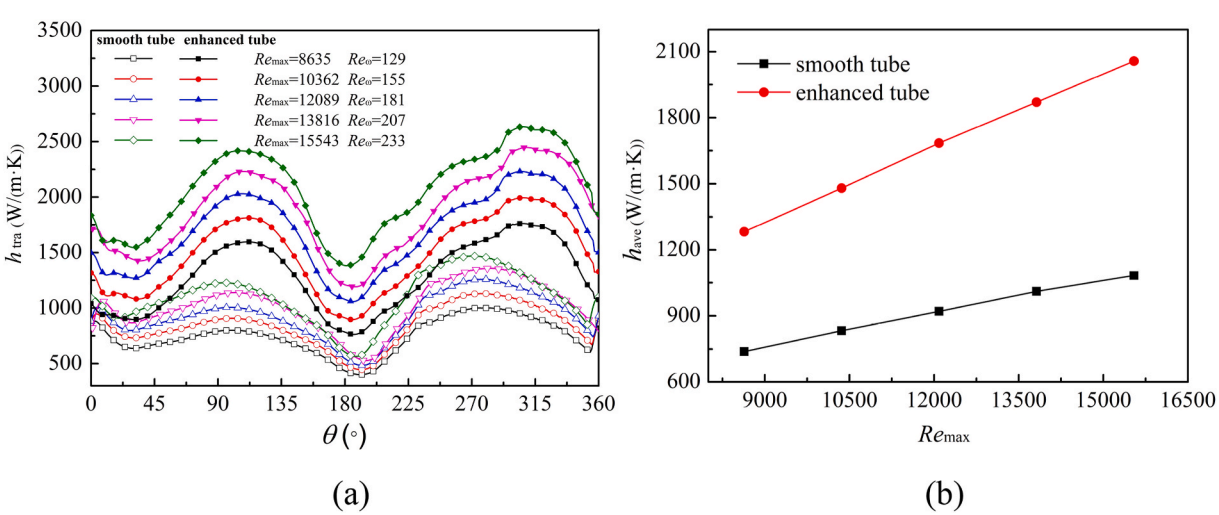

Fig. 9. The heat transfer coefficient of cooling tube for different Re_{max} and Re_{ω}: (a) transient heat transfer coefficient; (b) average heat transfer coefficient.

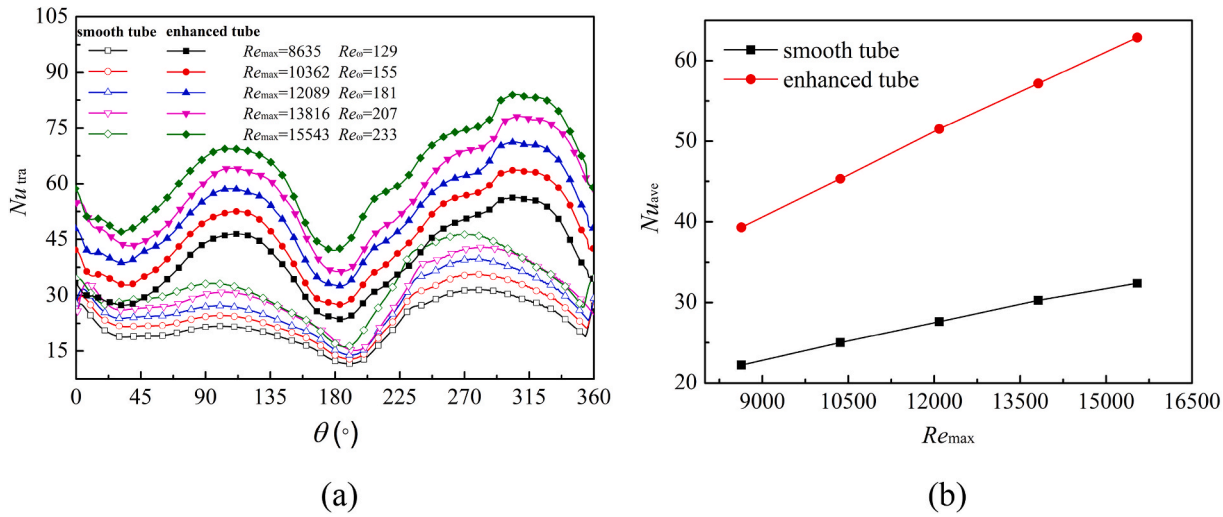

Fig. 10. The Nusselt number of cooling tube for different Re_{max} and Re_{ω}: (a) transient Nusselt number; (b) average Nusselt number.

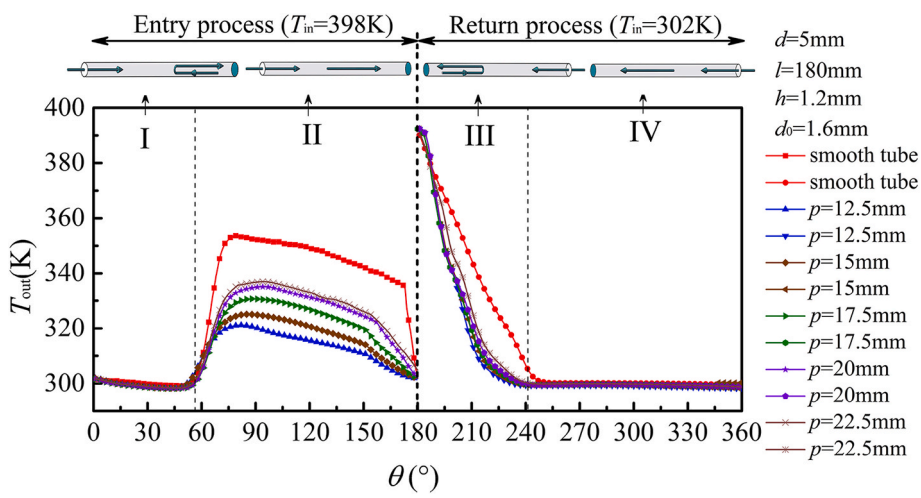

Fig. 11. The outlet temperature of fluid in cooling tube change with phase angle in different p for d = 5 mm, l = 180 mm, h = 1.2 mm, d_0 = 1.6 mm.

partial cooled fluid in the return process from the previous cycle remained in the cooling tube. This part of fluid was cooled by wall firstly and then flowed out of cooling tube during this stage. The temperature of this portion of fluid was low. Thus, the temperature drop range in stage I was small.

(2) In stage II, the fluid remained in the cooling tube which was from the return process of previous cycle had all flowed out of the outlet. The outlet fluid in stage II was all derived from the high temperature fluid which flowed from the regenerator end. The temperature of this part of fluid was high. Thus, the temperature drop range was large after cooling through the cooling tube.

(3) In stage III, the fluid began to flow from the compression chamber end to regenerator end along the cooling tube. However, part of cooled fluid in the entry process still remained in the cooling tube. This part of fluid firstly cooled by cooling wall and then flowed out of cooling tube during this stage. The temperature of this portion fluid was high. Thus, the temperature drop range in stage III was large.

(4) In stage IV, the fluid remained in the cooling tube from the entry process had all flowed out of outlet. The fluid flowing out of outlet in this stage was all derived from the low temperature fluid which flowed from the compression chamber end. Due to the low inlet temperature of this part of fluid, the temperature drop range was small after cooling through the cooling tube.

With the same tube diameter and length, the outlet temperature of fluid for enhanced tube was lower than that for smooth tube, especially in stages II and III. This indicates that the heat dissipation capability was significantly enhanced after inserting a helical wire into the cooling tube. The disturbance of wire to fluid increased with the decrease of helical pitch. Thus, stronger heat transfer was obtained with smaller helical pitch. In stages I and IV, the effect of wire on enhancing heat dissipation was not obvious. This is ascribed to the small temperature drop range from inlet fluid to wall.

The transient variation regularity of outlet temperature for smooth tube and enhanced tube with different d_0, h, d and l are shown in Fig. S4. The transient outlet temperature was similar for different d_0 in the range of this study (Fig. S4 (a)). In other words, when p and h were constant, the effect of d_0 on the outlet temperature of fluid was tiny. However, the effect of h on the outlet temperature of fluid was remarkable when the p and d_0 are constant (Fig. S4 (b)). The outlet temperature of fluid for enhanced tube decreased with the increase of h. The relatively large h was beneficial to enhance the heat transfer performance of the enhanced tube. Fig. S4 (c) shows that the outlet temperature of fluid decreased with the decrease of tube diameter. The cost of small tube diameter was

that the amount of cooling tube and the pressure drop increased under a constant flow rate. Thus, the material consumption and fabricating cost of cooling tube increased. In addition, the floor space of cooler increased and the compactness of Stirling engine deteriorated. Fig. S4 (d) shows that the outlet temperature of fluid decreased with the increase of tube length. However, the increase of tube length meant more material cost and higher pressure drop. Thus, the dead volume of Stirling engine increased and the output power for unit quality working fluid decreased. Therefore, it can effectively reduce the tube length, save the material cost, decrease the dead volume and improve the overall performance of Stirling engine by using the cooling tube with a helical wire.

Fig. 11 and Fig. S4 show the outlet temperature of fluid in cooling tube change with phase angle, which reflects the transient heat transfer performance of cooling tube. Fig. 12 shows the average outlet temperature of fluid change with the helical pitch of enhanced tube, the

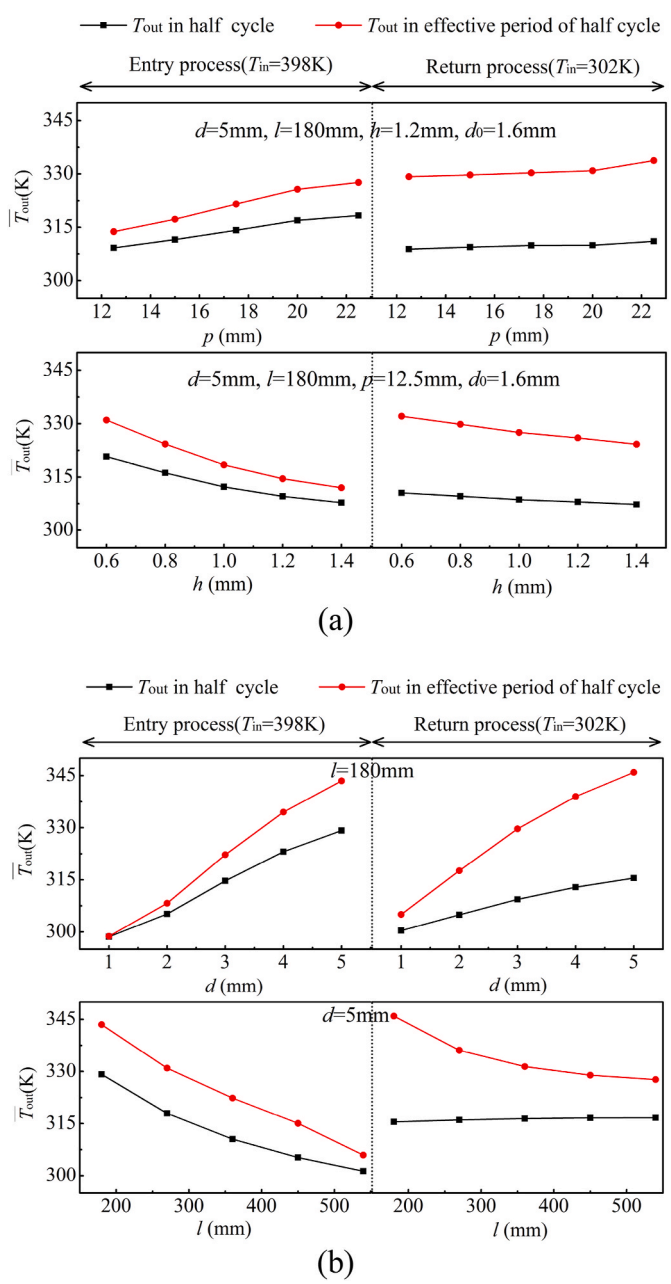

Fig. 12. The average outlet temperature in cooling tube change with geometric parameters: (a) change with p and h for enhanced tube; (b) change with d and l for smooth tube.

diameter and length of smooth tube. The black point and line represent the average outlet temperature of fluid over a half cycle during the entry process or the return process. The red point and line represent the average outlet temperature of fluid in stage II or III. As shown , with diameter of 5 mm and lengthen of 180 mm, the average temperature drop from inlet to outlet of enhanced tube ($p = 12.5$ mm, $h = 1.2$ mm, $d_0 = 1.6$ mm) was 1.29, 1.08, 1.54 and 1.32 times as much as that of smooth in entry process, return process, stage II and stage III, respectively.

The average outlet temperature of fluid increased with the increase of p for enhanced tube and diameter for smooth tube. It increased with the decrease of h for enhanced tube and length for smooth tube. The slope of the red line was larger than that of the black line. This suggests that the effects of helical pitch and height of enhanced tube as well as the diameter and length of smooth tube on the heat dissipation in the stage II or III were more significant than that in the entry or return process.

The average outlet temperature of fluid for the enhanced tube ($l = 180$ mm, $d = 5$ mm) with different helical pitches or heights was different. Fig. 13 shows the equivalent diameter or length of smooth tube at same average outlet temperature of the enhanced tube with different geometry parameters. The black histogram represents the average outlet temperature of entry or return process as the comparison standard, while the red histogram represents the average outlet temperature of stage II or III as the comparison standard. The top or the bottom half of Fig. 13 (a) shows the corresponding diameter or length sizes of smooth tube with $l = 180$ mm or $d = 5$ mm for the same average outlet temperature of enhanced tube with $l = 180$ mm, $d = 5$ mm, $h = 1.2$ mm under different helical pitch sizes. Fig. 13 (b) is similar to Fig. 13 (a), but the geometry parameters of enhanced tube was $l = 180$ mm, $d = 5$ mm, $p = 12.5$ mm under different height sizes.

As can be seen from Fig. 13, the dead volume of the enhanced tube can be significantly reduced when the same cooling performance was obtained as that of the smooth tube. For example, in the top half of Fig. 13 (a), when the length for smooth tube and enhanced tube was both 180 mm, the cooling effect of enhanced tube with helical pitch of 12.5 mm, height of 1.2 mm and diameter of 5 mm was equivalent to that of the smooth tube with diameter of 2.6 mm (52% of smooth tube). Thus, 3.7 times number of smooth tubes were needed to obtain same heat transfer performance over enhanced tube for a certain flow and velocity. As shown in the bottom half of Fig. 13 (a), when the diameter for smooth tube and enhanced tube was both 5 mm, the cooling effect of enhanced tube with helical pitch of 12.5 mm, height of 1.2 mm, and length of 180 mm was equivalent to that of smooth tube with length above 400 mm.

It can be seen from Figs. 12 and 13 that the heat dissipation capacity of enhanced tube was significantly larger than that of smooth tube with same tube diameter and length. From another perspective, the size and material consumption of enhanced tube were significantly less than the smooth tube with same heat dissipation capacity. Thus, the cooling tube with a helical wire applied in cooler can remarkably improve the efficiency and power, reduce consumables and improve the compactness for Stirling engine.

3.2. The friction factor and pressure drop

The transient friction factor change with phase angle for $Re_{max} = 13{,}816$, $Re_{\omega} = 207$ is shown in Fig. 14 (a). As shown, the resistance coefficient of enhanced tube was greater than that of smooth tube at most moments, while the resistance coefficient of the smooth tube is much greater than that of the enhanced tube near the moment of velocity reverse. This observation could be attributed to the following aspects:

The flow resistance will increase due to the addition of helical wire in the enhanced tube. Thus, the friction factor of enhanced tube was greater than that smooth tube in most of phase angle. At the moment of velocity reverse, there was no disturbance in the smooth tube, the

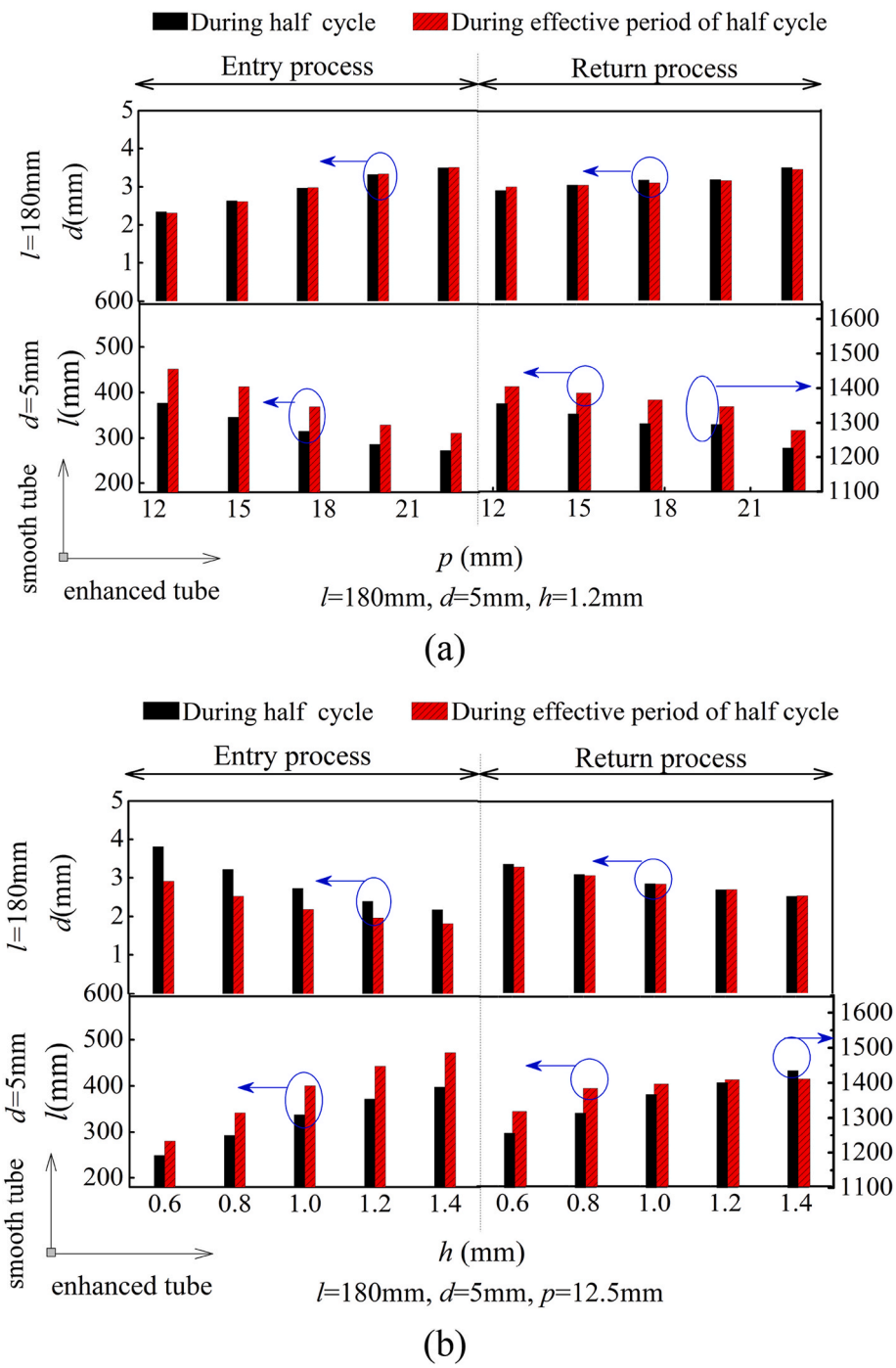

Fig. 13. The equivalent diameter or length of smooth tube at same average outlet temperature of the enhanced tube.

velocity magnitude was closed to 0 m/s. By the calculation formula of friction factor (formula 12), it can be seen that the friction factor at this time was extremely large. But for the enhanced tube, there were some flow (especially the radial flow) in the cooling tube even at the moment of velocity reverse due to the disturbance of helical wire. The overall velocity magnitude was not 0 m/s. Thus, the calculated value of the friction factor will not exist unusually large value.

To compare the flow expense of smooth tube with enhanced tube, the friction factor of cooling tube at phase angle of 90° change with Re_{max} was applied, as shown in Fig. 14 (b). The friction factor in phase angle of 90° slightly increased with the Re_{max} and the increase of amplitude for smooth tube was more obvious. The friction factor in phase angle of 90° for enhanced tube was larger than that for smooth tube. The pressure and pressure drop of smooth tube and enhanced tube will be further analyzed in the following part, as the flow resistance expense can not be fully reflected by the friction factor in a cycle especially near the reverse moment.

As shown in Fig. 15, the pressure distribution in the cooling tube was different at different phase angles, while the spatial distribution of pressure at a phase angle was uniform. The speed of pressure transmission was much faster than that of velocity and temperature. Therefore, the pressure contour plots in the cooling tube were basically the same when their inlet pressure values were the same (such as $\theta = 120°$ and $\theta = 240°$).

Although helical wire significantly enhanced the heat transfer capacity of cooling tube, the pressure drop might increase due to the flow

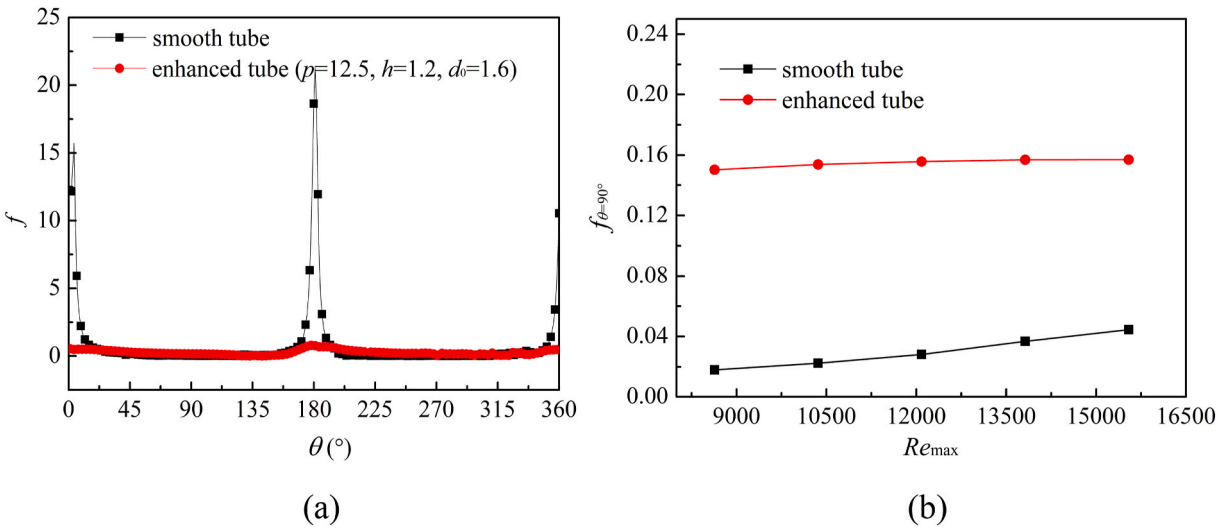

Fig. 14. The friction factor of cooling tube: (a) transient friction factor for Re_{max} = 13,816, Re_{ω} = 207; (b) the transient friction factor for θ = 90°.

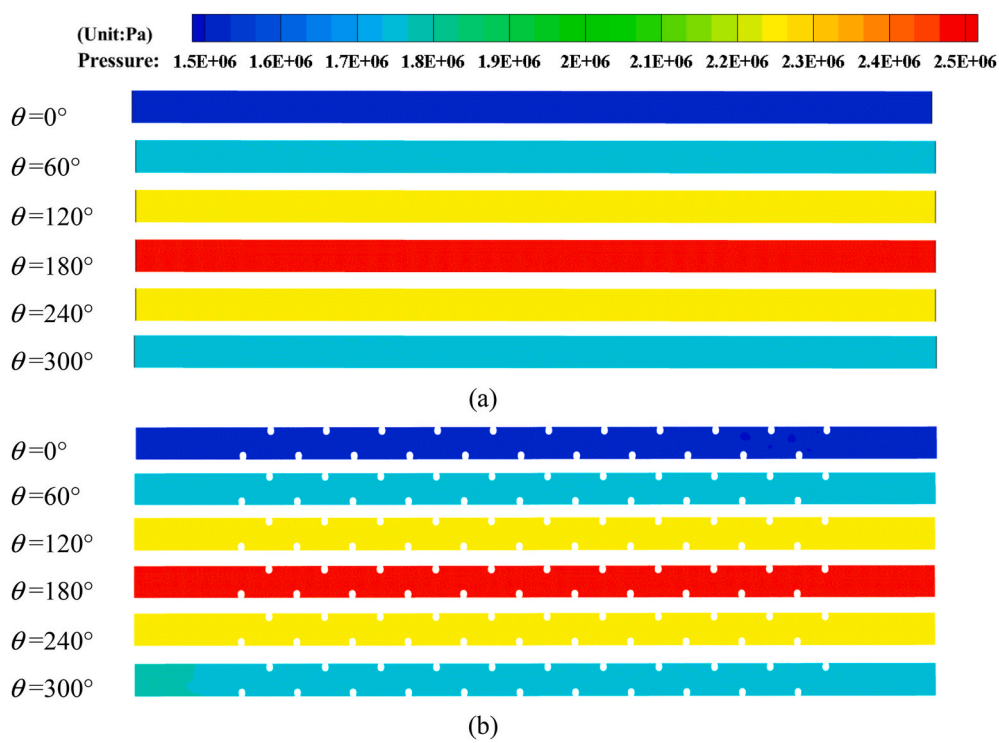

Fig. 15. The pressure contour plots of cooling tube in center axial cross section: (a) smooth tube; (b) enhanced tube.

hinder of helical disturbing device. However, Fig. 15 (a) and (b) show that the pressure contour plots of smooth tube and enhanced tube was similar. In other words, compared to the pressure variation with phase angle in cooling tube, the extra pressure drop by helical wire was almost negligible. Moreover, more complete pressure contour plots of cooling tube for different phase angles were shown in Fig. S5 in Supporting Information.

The quantitative change regularity of pressure with phase angle was shown in Fig. 16 The pressure changes of inlet and outlet were in accordance with cosine function, which was in the range of 1.5–2.5 MPa. The pressure curves for inlet and outlet were basically coincident. The absolute value of pressure difference from inlet to outlet was no more than 0.009 MPa, accounting for only 0.6% of the minimum pressure in the Stirling engine.

Fig. 17 shows the variation regularity of average absolute pressure difference from inlet to outlet change with d, l for the smooth tube and change with p, d_0, h for the enhanced tube. It can be seen that the pressure drop increased with the increase of l and decreased with the increase of d for smooth tube. With the same d and l, the pressure drop increased with the decrease of p and the increase of h for enhanced tube. The effect of d_0 on the pressure drop was relatively small compared with h or p. However, even when the p was 12.5 mm and h was 1.2 mm for enhanced tube, the average absolute value of pressure drop from inlet to outlet was only 0.00448 MPa, 0.003956 MPa higher than that for smooth tube, which accounted for only 0.26% of the minimum pressure in the Stirling engine.

The main heat exchangers in the Stirling engine include a regenerator, a heater and a cooler. The regenerator acts like a thermal sponge

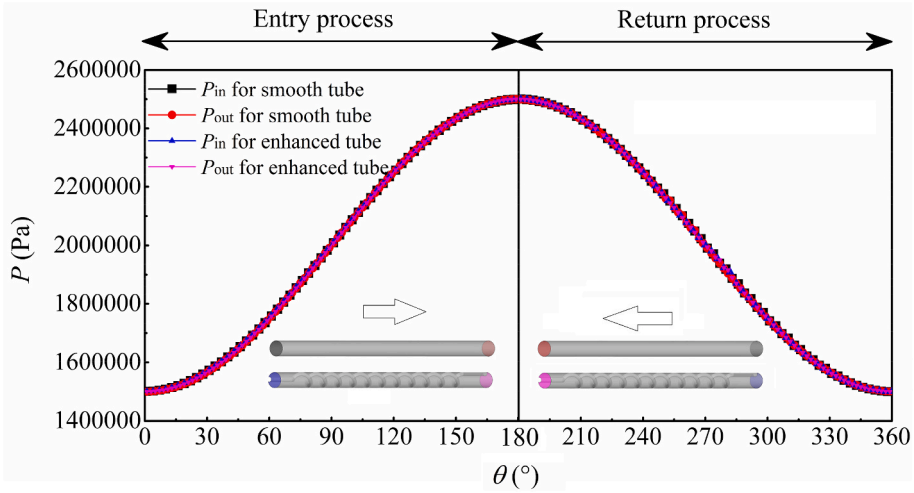

Fig. 16. The inlet and outlet pressure of cooling tube change with phase angle.

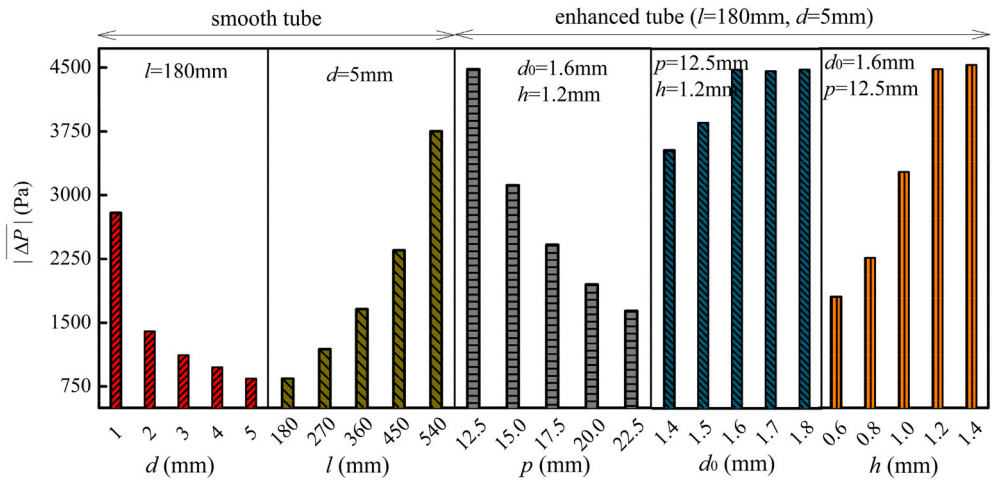

Fig. 17. The average absolute pressure difference of cooling tube from inlet and outlet change with d, l for the smooth tube and change with p, d_0, h for the enhanced tube.

that absorbs and releases heat alternatively inside the Stirling engine. In order to obtain an excellent endothermic and exothermic capacity, the porous structure, such as the stack wire mesh, was widely used in regenerator. It occupied the vast majority of the pressure drop of Stirling engine. As shown in Fig. 18, the pressure drop characteristics of the stainless steel wire mesh were studied in literature [48]. The results show that the maximum pressure drop in a cycle was 60,000 Pa and the average pressure drop in a cycle was 35,517 Pa. Wang studied the pressure drop characteristics of the wire mesh regenerator using a local nonthermal equilibrium model [49]. The results show that the maximum pressure drop and the average pressure drop in a cycle was 63,000 Pa and 40,107 Pa, respectively. In this study, even for the enhanced cooling tube with the $p = 12.5$ mm, $h = 1.2$ mm, $d_0 = 1.6$ mm, the maximum pressure drop from inlet to outlet was only about 9000 Pa, and the average pressure drop in a cycle was 4480 Pa, which was 7835 Pa and 3856 Pa more than that of the smooth tube, respectively. The extra pressure drop of the enhanced cooling tube accounted for 12.4–13.1% of the maximum pressure drop of regenerator, and 9.6–10.9% of the average pressure drop of regenerator. Therefore, compared to smooth tube, the pressure drop increment of the enhanced cooling tube proposed in this manuscript was inapparent for the whole pressure drop of Stirling engine system.

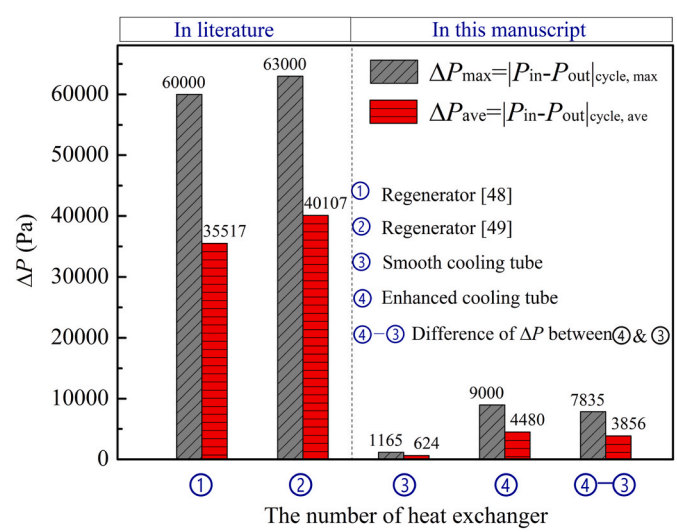

Fig. 18. The comparison of pressure drop of the cooling tube in this work (enhanced tube for $p = 12.5$ mm, $h = 1.2$ mm, $d_0 = 1.6$ mm, $l = 180$ mm, $d = 5$ mm and smooth tube for $l = 180$ mm, $d = 5$ mm) with a regenerator in literatures.

4. Conclusions

The heat transfer of cooling tube in Stirling engine was enhanced by using helical wire. The advantages of enhanced tube were evaluated by the decrease of outlet temperature or the reduction of cooler size. Compared with the evaluation methodology of *PEC* based on steady unidirectional flow, this evaluation methodology was more practical for Stirling engine cooling tube. The main conclusions are as follows:

(1) The streamline in enhanced tube was helical, which promoted the heat transfer between boundary fluid and core area fluid. The temperature boundary layer near the wall surface was thinned as well. The temperature homogeneity of fluid and the heat dissipation capability was enhanced. With the same boundary conditions, the heat of fluid can be quickly discharged out of the enhanced tube. Therefore, the temperature of fluid flowing into the compression chamber was decreased, and the cold end temperature of thermodynamic cycle for Stirling engine was reduced.

(2) The transient heat transfer performance of the cooling tube changed all the time in a flow cycle. The transient and average heat transfer coefficient and *Nu* number of the cooling tube increased with the $Re_{\max}$ and Re_{ω} number. The increase amplitude of the enhanced tube was significantly larger than that of the smooth tube. The disturbance of wire to fluid increased with the decrease of p and the increase of h, while the effect of d_0 is small. The small p and large h of helical wire contributed to the heat dissipation of enhanced tube. For smooth tube, there were two ways to achieve the same heat dissipation effect as enhanced tube: reducing tube diameter accompanied with increasing tubes amount or increasing tube length. But the dead volume of Stirling engine would be remarkably increased by these methods. Thus, the enhanced tube can enhance the compactness of Stirling engine.

(3) The flow of working gas can be hindered by the helical wire in enhanced tube, which increased the pressure drop of cooling tube. However, the maximum and average pressure drop of enhanced tube only accounted for 0.6% and 0.26% of the minimum pressure in the Stirling engine (1.5 MPa). Compared to smooth tube, the extra pressure drop of enhanced tube only accounted for 9.6–13.1% of the pressure drop of a regenerator. Thus, the cost of enhanced cooling tube is small and its benefits is prominent.

Declaration of competing interest

The authors declare that they have no known competing financial interests or personal relationships that could have appeared to influence the work reported in this paper.

Acknowledgements

This research was supported by the National Natural Science Foundation of China (51736004), the Natural Science Foundation of Hunan Province, China (2020JJ5590), the Research Foundation of Educational Department of Hunan Province, China (19C0084), the Key Laboratory of Renewable Energy Electric-Technology of Hunan Province (2019ZNDL004), the Innovative Team of Key Technologies of Energy Conservation, Emission Reduction and Intelligent Control for Power-Generating Equipment and System, CSUST.

Appendix A. Supplementary data

Supplementary data to this article can be found online at https://doi.org/10.1016/j.ijthermalsci.2021.107063.

Nomenclature

c_p	specific heat (J kg^{-1} K^{-1})
d	inner diameter of heating tube (mm)
d_0	diameter of wire (mm)
F_1	blending function
f	friction factor
h	helical wire height in the vertical section (mm); heat transfer coefficient (W m^{-1} K^{-1})
k	turbulent kinetic energy (m^2 s^{-2})
l	overall length (mm)
l_1	end length (mm)
P	pressure (Pa)
p	pitch of helical wire (mm)
P_0	average pressure in a cycle (Pa)
P_1	amplitude of pressure in a cycle (Pa)
$\widetilde{P}_k$	production limiter to prevent the build-up of turbulence in stagnation regions (kg^2 m^{-1} s^{-3})
q	heat flux (W/m^2)
r	radial position (mm)
R	radius (mm)
Re_{ω}	kinetic Reynolds number, similar to the Reynolds number in steady flow
$Re_{\max}$	maximum Reynolds number, dimensionless frequency
S	invariant measure of the strain rate (s^{-1})
t	time (s)
T	temperature (K)
u	velocity (m s^{-1})
$u_{\mathrm{m},\max}$	amplitude of bulk mean velocity (m s^{-1})
z	axial position (mm)

Greek symbols

α	blending constant
β	blending constant
Δ	difference value
Φ	energy dissipation due to viscosity (W m^{-3})
λ	thermal conductivity (W m^{-1} k^{-1})
μ	dynamic viscosity (kg m^{-1} s^{-1})
μ_t	turbulent dynamic viscosity (kg m^{-1} s^{-1})
ν	kinematic viscosity (m^2 s^{-1})
θ	phase angle (°)
ρ	density (kg m^{-3})
σ	blending constant
ω	specific dissipation rate(s^{-1}) or angular velocity (rad s^{-1})

subscripts

i	tensor
in	inlet
out	outlet
w	wall
ave	average
m	average
max	maximum

References

[1] A. Abuelyamen, R. Ben-Mansour, Energy efficiency comparison of Stirling engine types (α, β, and γ) using detailed CFD modeling, Int. J. Therm. Sci. 132 (2018) 411–423.

[2] B.J.G. de la Bat, R.T. Dobson, T.M. Harms, A.J. Bell, Simulation, manufacture and experimental validation of a novel single-acting free-piston Stirling engine electric generator, Appl. Energy 263 (2020) 1–20.

[3] F. Ahmed, H. Hulin, A.M. Khan, Numerical modeling and optimization of beta-type Stirling engine, Appl. Therm. Eng. 149 (2019) 385–400.

[4] D. Dai, F. Yuan, R. Long, Z. Liu, W. Liu, Performance analysis and multi-objective optimization of a Stirling engine based on MOPSOCD, Int. J. Therm. Sci. 124 (2018) 399–406.

[5] W. Uchman, L. Remiorz, K. Grzywnowicz, J. Kotowicz, Parametric analysis of a beta Stirling engine–A prime mover for distributed generation, Appl. Therm. Eng. 145 (2018) 693–704.

[6] G. Xiao, U. Sultan, M. Ni, H. Peng, X. Zhou, S. Wang, Z. Luo, Design optimization with computational fluid dynamic analysis of β-type Stirling engine, Appl. Therm. Eng. 113 (2017) 87–102.

[7] D. Ipci, H. Karabulut, Thermodynamic and dynamic analysis of an alpha type Stirling engine and numerical treatment, Energy Convers. Manag. 169 (2018) 34–44.

[8] F. Aksoy, H. Solmaz, H. Karabulut, C. Cinar, Y.O. Ozgoren, S. Polat, A thermodynamic approach to compare the performance of rhombic-drive and crank-drive mechanisms for a beta-type Stirling engine, Appl. Therm. Eng. 93 (2016) 359–367.

[9] P.V. Trevizoli, J.R. Barbosa, Thermal-hydraulic behavior and influence of carryover losses in oscillating-flow regenerators, Int. J. Therm. Sci. 113 (2017) 89–99.

[10] Z. Li, Y. Haramura, D. Tang, C. Guo, Analysis on the heat transfer characteristics of a micro-channel type porous-sheets Stirling regenerator, Int. J. Therm. Sci. 94 (2015) 37–49.

[11] Z. Song, J. Chen, L. Yang, Heat transfer enhancement in tubular heater of Stirling engine for waste heat recovery from flue gas using steel wool, Appl. Therm. Eng. 87 (2015) 499–504.

[12] N. Hirao, M. Komura, Improvement in specific power of stirling engine by using a new heat exchanger, J. Jpn. Inst. Energy 88 (2009) 1095–1100.

[13] S.J. Tang, Performance Investigations on Radiation Cooler of Free-Piston Stirling Engine, Nanjing University of Aeronautics and Astronautics, 2016.

[14] M.H. Pourrezaei, M.R. Malayeri, K. Hooman, Thermal performance and mechanisms of soot deposition in foam structured exhaust gas recirculation coolers, Int. J. Therm. Sci. 146 (2019) 106108.

[15] H. Sadighi Dizaji, S. Jafarmadar, S. Khalilarya, S. Pourhedayat, A comprehensive exergy analysis of a prototype Peltier air-cooler; experimental investigation, Renew. Energy 131 (2019) 308–317.

[16] L. Zhu, J. Yu, Optimization of heat sink of thermoelectric cooler using entropy generation analysis, Int. J. Therm. Sci. 118 (2017) 168–175.

[17] A. Dehghan, A.K. Valian, A. Batooei, H. Saberinejad, Numerical investigation of reciprocating flow in a shell and tube heat exchanger used as a cooler in gamma Stirling engine, Modares Mech. Eng. 17 (2017) 359–366.

[18] M. Kanzaka, M. Iwabuchi, Study on heat transfer of heat exchangers in the Stirling engine: performance of heat exchangers in the test Stirling engine, JSME Int. J. 35 (1992) 647–652.

[19] S. Alfarawi, R. AL-Dadah, S. Mahmoud, Influence of phase angle and dead volume on gamma-type Stirling engine power using CFD simulation, Energy Convers. Manag. 124 (2016) 130–140.

[20] D.G. Thombare, S.K. Verma, Technological development in the Stirling cycle engines, Renew. Sustain. Energy Rev. 12 (2008) 1–38.

[21] A.E. Bergles, Some perspectives on enhanced heat transfer second generation heat transfer technology, ASME J. Heat Transf. 110 (1988) 1082–1096.

[22] R.L. Webb, Heat transfer enhancement second generation technology, Mech. Eng. 115 (1983) 60–67.

[23] Z.Y. Guo, W.Q. Tao, R.K. Shah, The field synergy (coordination) principle and its applications in enhancing single phase convective heat transfer, Int. J. Heat Mass Tran. 48 (2005) 1797–1807.

[24] J.M. Wu, W.Q. Tao, Investigation on laminar convection heat transfer in fin-and-tube heat exchanger in aligned arrangement with longitudinal vortex generator from the viewpoint of field synergy principle, Appl. Therm. Eng. 27 (2007) 2609–2617.

[25] A. Bejan, P.A. Pfister, Evaluation of heat transfer augmentation techniques based on their impact on entropy generation, Lett. Heat Mass Tran. 7 (1980) 97–106.

[26] L. Chen, A. Yang, Z. Xie, F. Sun, Constructal entropy generation rate minimization for cylindrical pin-fin heat sinks, Int. J. Therm. Sci. 111 (2017) 168–174.

[27] W. Liu, P. Liu, J.B. Wang, N.B. Zheng, Z.C. Liu, Exergy destruction minimization: a principle to convective heat transfer enhancement, Int. J. Heat Mass Tran. 122 (2018) 11–21.

[28] N. Zheng, P. Liu, F. Shan, Z. Liu, W. Liu, Turbulent flow and heat transfer enhancement in a heat exchanger tube fitted with novel discrete inclined grooves, Int. J. Therm. Sci. 111 (2017) 289–300.

[29] O. Keklikcioglu, V. Ozceyhan, Experimental investigation on heat transfer enhancement in a circular tube with equilateral triangle cross sectioned coiled-wire inserts, Appl. Therm. Eng. 131 (2018) 686–695.

[30] H. Bas, V. Ozceyhan, Heat transfer enhancement in a tube with twisted tape inserts placed separately from the tube wall, Exp. Therm. Fluid Sci. 41 (2012) 51–58.

[31] J.G. Jiang, Z.X. Yuan, G.D. Xia, Periodical heat transfer in parallel-plate channel of improved flow-inclining inserts, Int. J. Therm. Sci. 48 (2009) 1748–1754.

[32] W. Wang, Y. Zhang, B. Li, H. Han, X. Gao, Influence of geometrical parameters on turbulent flow and heat transfer characteristics in outward helically corrugated tubes, Energy Convers. Manag. 136 (2017) 294–306.

[33] M. Kuosa, K. Saari, A. Kankkunen, T.M. Tveit, Oscillating flow in a stirling engine heat exchanger, Appl. Therm. Eng. 45–46 (2012) 15–23.

[34] Z.L. Qi, Q.J. Wan, X.D. Zhang, H.L. Huang, Heat exchange performance of Stirling engine heat exchanger, J. Eng. Thermophys. 35 (6) (2014) 1144–1147.

[35] S.J. Tang, H.L. Huang, Y. Zhang, Performance investigations on radiation cooler of Stirling engine, in: China Engineering Thermophysics Conference, Dalian, China, October 30 -November 2, 2015, p. 153520.

[36] P. Liu, N. Zheng, F. Shan, Z. Liu, W. Liu, Heat transfer enhancement for laminar flow in a tube using bidirectional conical strip inserts, Int. J. Heat Mass Tran. 127 (2018) 1064–1076.

[37] K. Sharifi, M. Sabeti, M. Rafiei, A.H. Mohammadi, L. Shirazi, Computational fluid dynamics (CFD) technique to study the effects of helical wire inserts on heat transfer and pressure drop in a double pipe heat exchanger, Appl. Therm. Eng. 128 (2018) 898–910.

[38] D. Muñoz-Esparza, E. Sanmiguel-Rojas, Numerical simulations of the laminar flow in pipes with wire coil inserts, Comput. Fluids 44 (2011) 169–177.

[39] J.P. Solano, R. Herrero, S. Espín, A.N. Phan, A.P. Harvey, Numerical study of the flow pattern and heat transfer enhancement in oscillatory baffled reactors with helical coil inserts, Chem. Eng. Res. Des. 90 (2012) 732–742.
[40] J.R. McDonough, S.M.R. Ahmed, A.N. Phan, A.P. Harvey, A study of the flow structures generated by oscillating flows in a helical baffled tube, Chem. Eng. Sci. 171 (2017) 160–178.
[41] A. García, P.G. Vicente, A. Viedma, Experimental study of heat transfer enhancement with wire coil inserts in laminar-transition-turbulent regimes at different Prandtl numbers, Int. J. Heat Mass Tran. 48 (2005) 4640–4651.
[42] V.D. Zimparov, P.J. Penchev, Performance evaluation of some tube inserts as heat transfer enhancement techniques, Heat Tran. Eng. 27 (2006) 39–46.
[43] F. Xin, Z. Liu, S. Wang, W. Liu, Study of heat transfer in oscillatory flow for a Stirling engine heating tube inserted with spiral spring, Appl. Therm. Eng. 143 (2018) 182–192.
[44] F. Xin, Z. Liu, N. Zheng, P. Liu, W. Liu, Numerical study on flow characteristics and heat transfer enhancement of oscillatory flow in a spirally corrugated tube, Int. J. Heat Mass Tran. 127 (2018) 402–413.
[45] F.R. Menter, M. Kuntz, R. Langtry, Ten years of industrial experience with the SST turbulence model, Turb., Heat Mass Transf. 4 (2003) 625–632.
[46] G. Xiao, T. Zhou, M. Ni, C. Chen, Z. Luo, K. Cen, Study on oscillating flow of moderate kinetic Reynolds numbers using complex velocity model and phase Doppler anemometer, Appl. Energy 130 (2014) 830–837.
[47] T.X. Zhou, Study on Oscillating Flow and Heat Transfer Characteristics in Heated Pine of Stirling Engine, Zhejiang University, 2014.
[48] R.X. Jiang, Research on Flow and Heat Transfer Characteristics of Regenerator in Stirling Engine, Nanjing University of Aeronautics and Astronautics, 2014.
[49] S. Wang, F. Xin, Z.C. Liu, W. Liu, Research on flow and heat transfer characteristics of Stirling engine regenerator, in: China Engineering Thermophysics Conference, Suzhou, China, October 27-30, 2017.